Journal of Sound and Vibration (1998) **209**(5), 707–722

INSIGHT INTO THE SENSITIVITY TO AXIAL COMPRESSIVE LOAD OF THE NATURAL FREQUENCIES OF STRUCTURES WHICH INCLUDE SHEAR DEFORMATION

P. N. Bennett and F. W. Williams

Division of Structural Engineering, Cardiff School of Engineering, University of Wales Cardiff, Queens Buildings, P.O. Box 686, *Cardiff CF*2 3*TB, Wales*

(*Received* 12 *March* 1997, *and in final form* 26 *June* 1997)

The effect is considered of transverse shear deformation and rotatory inertia on the natural frequencies of loaded structures. The paper covers the many structures for which there is a linear or nearly linear relationship between the square of the natural frequencies and load factor regardless of whether or not shear deformation is included. Equations are derived and evaluated for predicting and/or correcting the errors caused by neglecting the shear deformation of such structures when calculating their natural frequencies under load. The equations are shown to give good predictions of the exact results for axially compressed prismatic plate assemblies, including two sandwich panels with low core density and shear stiffnesses. The equations, their results and the stiffened panel examples are presented so as to give qualitative insight and numerical guidance both on the consequences of neglecting shear deformation (and rotatory inertia) and on the accuracy of the simple correction formulas presented. In particular, they show that the percentage errors caused by neglecting shear deformation when calculating natural frequencies of loaded structures will be greater—often very much greater—than the percentage errors in unloaded natural frequencies or buckling loads caused by neglecting shear deformation.

© 1998 Academic Press Limited

1. INTRODUCTION

There is a substantial range of structures, e.g., frames and stiffened plate structures, for which each natural frequency of free vibration n varies with the load level σ (= load factor or uniform compressive stress depending upon the problem) either exactly or to a good approximation according to the equation [1, 2]

$$\frac{n^2}{n_{rc}^2} + \frac{\sigma}{\sigma_{rc}} = 1, \tag{1}$$

where n_{rc} and σ_{rc} are the rth unloaded natural frequency and the corresponding buckling load factor or stress, respectively. Here "corresponding" means that the vibrational and buckling modes are identical or similar and the subscript c has been introduced because it is used later. The solid line of Figure 1 shows this linear relationship between n^2 and σ graphically.

Many previous papers have considered the effect of load level on the natural frequencies of free vibration of structures. Cases considered include the effect of axial compressive loading on the natural frequencies of Bernoulli–Euler and Timoshenko beams [3–7], thin rectangular plates and prismatic assemblies of thin plates [8–15]. Fewer authors have

0022–460X/98/050707 + 16 $25.00/0/sv971185 © 1998 Academic Press Limited

considered the effect of transverse shear deformation and rotatory inertia on the natural frequencies of in-plane loaded thick plates [16–20].

Of the above papers, only in references [4, 5, 11, 13] has the linear relationship of equation (1) been plotted as either exactly or approximately true. From, e.g., reference [21], equation (1) is known to apply exactly to several types of individual members, including simply supported Bernoulli–Euler, Timoshenko and Vlasov beams, as well as to thin flat rectangular plates which are simply supported at their ends. The relationship has also been shown [22, 23] to hold exactly for a family of thin, flat-walled structures which can be modelled as assemblies of thin rectangular plates interconnected along their longitudinal edges and simply supported at their ends.

The solid line in Figure 1 is assumed to have been calculated with shear deflection ignored; e.g., Bernoulli beam theory or classical plate theory (CPT) is used. The dashed line in Figure 1 represents an (actually or assumed) linear relationship between n^2 and σ when shear deflection is taken into account; e.g., Timoshenko theory is used for the beam case or shear deformable plate theory (SDPT) is used for the plate case. The values of α_n and σ_σ shown in Figure 1 are given by

$$\alpha_n = n_{rs}^2 / n_{rc}^2, \qquad \alpha_\sigma = \sigma_{rs} / \sigma_{rc}. \tag{2}$$

Here the subscript s denotes that shear deflection has been included (e.g., SDPT has been used in the case of plates) and subscript c denotes its omission (e.g., CPT has been used for plates or Bernoulli–Euler theory has been used for beams). Shear deflection must reduce natural frequencies and buckling load factors, and so $\alpha_n < 1$ and $\alpha_\sigma < 1$. Since rotatory inertia affects n_{rs} but not σ_{rs}, $\alpha_n < \alpha_\sigma < 1$ is to be expected and occurs for all results known to the authors.

The main physical insights and conclusions of the present paper are applicable to any structure or individual member for which the two straight lines of Figure 1 are exact or reasonably close representations of the behaviour with shear deflection respectively neglected or included. However, the examples presented are only for the very important case of prismatic assemblies of thin plates which are simply supported at their ends; e.g., aerospace wing panels. It is shown below that Figure 1 explains the sensitivity to longitudinally compressive load of the error caused by neglecting shear deformation when calculating natural frequencies; e.g., by using CPT instead of SDPT. This both gives physical insight and also enables predictions to be made by simple formulas which are accurate enough for many design purposes, as is proved by the comparisons with the (almost) exact results for the examples presented.

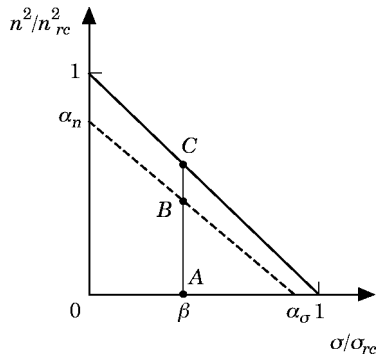

Figure 1. The linear relationship between the squared natural frequency and the critical buckling stress for CPT (—) and SDPT (---), showing the definitions of α_n and α_σ.

2. PREDICTION OF ERRORS DUE TO IGNORING SHEAR DEFORMATION WHEN CALCULATING NATURAL FREQUENCIES OF LOADED STRUCTURES, ILLUSTRATED BY PRISMATIC PLATE ASSEMBLIES

Up to the end of the paragraph containing equation (7), this section gives the background on the prismatic plate assemblies used to illustrate the method. It can be omitted if desired. It has been shown [24] that for uniformly compressed plates, or prismatic assemblies of isotropic plates [22], with simply supported ends, the frequency n and the longitudinal compressive stress σ always occur together in the combination $(\sigma + 4\rho\lambda^2 n^2)$ when assembling the CPT dynamic stiffness matrix for any given value of the longitudinal half-wavelength λ. Hence it was determined [24] that if, for any chosen value of λ, n_{rc} was the rth of the CPT natural frequencies of an unloaded isotropic assembly of density ρ, then the panel would possess an *identical* mode of buckling under uniform longitudinal compressive stress σ_{rc} given by

$$\sigma_{rc} = 4\rho\lambda^2 n_{rc}^2. \tag{3}$$

Here the subscript c denotes the use of CPT. Hence, *for the same value of* λ, the natural frequencies, $n_{\sigma rc}$, of such an assembly when subjected to a uniform longitudinally invariant stress σ can be obtained from the unloaded natural frequencies as [22]

$$n_{\sigma rc}^2 = n_{rc}^2 - \sigma/(4\rho\lambda^2). \tag{4}$$

Combining equations (3) and (4) gives

$$\frac{n_{\sigma rc}^2}{n_{rc}^2} = 1 - \frac{\sigma}{\sigma_{rc}}, \tag{5}$$

which is essentially equation (1).

From the governing equations for SDPT (see equation (1) of reference [25]) it can be seen that, for the commonest case in which the longitudinally compressive loads for the plates are assumed to be acting at their neutral surfaces, the first moment of mass of the cross-section (m_1) will be zero and, consequently, many of the applied load and natural frequency terms occur in the correct combination for the SDPT equivalent of equation (4) to hold; i.e., they appear in the combination $(\sigma + 4\rho\lambda^2 n^2)$. However, one or more other combinations of σ and n also occur, e.g., involving the second moment of mass of the plate cross-section, and so the SDPT equivalent of equations (3) and (4) cannot be used to convert between the SDPT critical buckling stresses and SDPT frequencies exactly. Nevertheless, because the combination $(\sigma + 4\rho\lambda^2 n^2)$ occurs it is reasonable to hypothesize that the SDPT equivalent of equation (4) may be a sufficiently good approximation for many purposes, so that equations (3) and (4) can be rewritten for SDPT as

$$\sigma_{rs} \approx 4\rho\lambda^2 n_{rs}^2 \qquad \text{and} \qquad n_{\sigma rs}^2 \approx n_{rs}^2 - \sigma/(4\rho\lambda^2). \tag{6, 7}$$

This hypothesis is adopted throughout this paper and its validity is explored and largely justified by comparison with (almost) exact results given in sections 4 and 5.

The linear relationship between n^2 and σ obtained when using CPT is shown as the solid straight line in Figure 1, and CPT and SDPT are interpreted loosely in the rest of sections 2 and 3 to indicate, respectively, the omission or inclusion of shear deformation for any type of structure; e.g., plane frames as well as prismatic plate assemblies. The ratios α_n and α_σ of equation (2) can, if known, be used to construct the dashed line shown on Figure 1.

Let

$$\beta = \sigma/\sigma_{rc}. \tag{8}$$

Then it can be seen from Figure 1 that

$$AC = n_{\sigma rc}^2, \qquad AB = n_{\sigma rs}^2, \tag{9}$$

where c and s denote CPT and SDPT and r denotes the rth natural frequency n in the presence of the load factor or stress σ. Hence ε, the percentage error caused by using CPT to calculate $n_{\sigma rs}^2$, is defined as follows:

$$\varepsilon = 100\left(\frac{BC}{AB}\right) = 100\left(\frac{AC - AB}{AB}\right) = 100\left\{\left(\frac{n_{\sigma rc}}{n_{\sigma rs}}\right)^2 - 1\right\}; \tag{10}$$

i.e., $n_{\sigma rc}^2$ will be too high by this percentage, and the percentage correction, δ, required to obtain $n_{\sigma rs}^2$ from $n_{\sigma rc}^2$, is given by

$$\delta = -100\left(\frac{BC}{AC}\right) = -100\left(\frac{AC - AB}{AC}\right) = -100\left\{1 - \left(\frac{n_{\sigma rs}}{n_{\sigma rc}}\right)^2\right\}. \tag{11}$$

Equations (1) or (5) and (8) give

$$\left(\frac{n_{\sigma rc}}{n_{rc}}\right)^2 = \left(1 - \frac{\sigma}{\sigma_{rc}}\right) = 1 - \beta. \tag{12}$$

Similarly, for the SDPT case, substituting equation (6) in equation (7) (or, alternatively, the dashed straight line of Figure 1 if the structure is not a prismatic plate assembly) gives

$$\left(\frac{n_{\sigma rs}}{n_{rs}}\right)^2 \approx \left(1 - \frac{\sigma}{\sigma_{rs}}\right). \tag{13}$$

Substituting equation (2) into equation (13) and then using equation (8) gives

$$\left(\frac{n_{\sigma rs}}{n_{rc}}\right)^2 \frac{1}{\alpha_n} \approx \left(1 - \frac{\sigma}{\alpha_\sigma\, \sigma_{rc}}\right) = 1 - \frac{\beta}{\alpha_\sigma}; \tag{14}$$

i.e.,

$$\left(\frac{n_{\sigma rs}}{n_{rc}}\right)^2 \approx \alpha_n \left(1 - \frac{\beta}{\alpha_\sigma}\right). \tag{15}$$

Dividing equation (12) by equation (15) gives

$$\left(\frac{n_{\sigma rc}}{n_{\sigma rs}}\right)^2 \approx \frac{1 - \beta}{\alpha_n\,(1 - \beta/\alpha_\sigma)}. \tag{16}$$

Hence the percentage error of the CPT frequencies, ε, is given by equations (10) and (16) as

$$\varepsilon = 100\left\{\left(\frac{n_{\sigma rc}}{n_{\sigma rs}}\right)^2 - 1\right\} \approx 100\left\{\frac{(1 - \beta)}{\alpha_n\,(1 - \beta/\alpha_\sigma)} - 1\right\} \tag{17}$$

and the percentage correction needed to CPT is given by equations (11) and (16) as

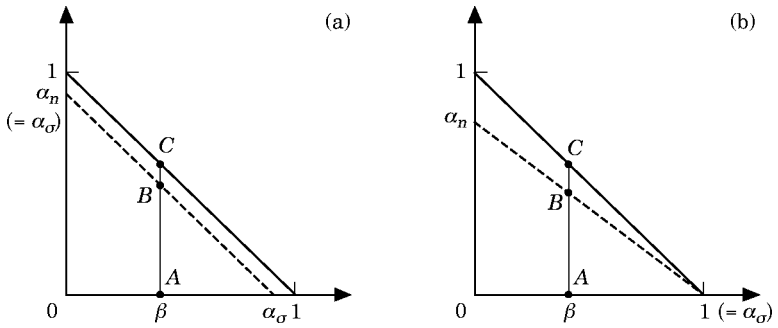

Figure 2. The limiting cases of Figure 1 for the hypothesis that $\alpha_n \leqslant \alpha_\sigma$.

$$\delta = -100\left\{1 - \left(\frac{n_{\sigma rs}}{n_{\sigma rc}}\right)^2\right\} \approx -100\left\{1 - \frac{\alpha_n\,(1 - \beta/\alpha_\sigma)}{(1 - \beta)}\right\}. \tag{18}$$

Note particularly that only equations (3)–(7) are specific to prismatic plate assemblies, whereas equations (1), (2) and (8)–(18) (and also equations (19)–(23) below) all apply to any structure for which σ and the square of the natural frequencies are approximately linearly related both with and without shear deformation included; i.e., equation (12) is approximately true and equation (13) holds.

3. SOME OF THE PHYSICAL INSIGHTS OBTAINABLE FROM FIGURE 1

Many qualitative insights for any structure for which the load factor or stress σ is linearly related, or approximately linearly related, to n^2, i.e., to the square of any chosen natural frequency of the structure, are given in Figure 1. The simple equations derived from Figure 1 in section 2 also enable very helpful "back of the envelope" calculations to be made. These give exact numerical predictions of ε and δ when the two straight lines of Figure 1 exactly represent the behaviour of the structure and give useful approximate numerical predictions of ε and δ when the true curves for the structure with and without shear deformation included are reasonably close to, respectively, the dashed and solid straight lines of Figure 1. Some of these insights and numerical predictions are discussed in this section.

On the hypothesis promulgated above that $\alpha_n < \alpha_\sigma$, and remembering that $\alpha_n < 1$ and $\alpha_\sigma < 1$, in Figure 2 are represented the two limiting cases of $\alpha_n = \alpha_\sigma$ and $\alpha_\sigma = 1$. Conclusions that hold for *both* of these cases in the following discussion will hold for any possible combinations of α_n and α_σ.

The percentage error ε obtained by ignoring shear deflection is $100 \times (BC/AB)$; see equation (10). For Figure 2(a), BC is constant as β is increased, because the solid and dashed lines are parallel, while AB decreases monotonically. Hence ε increases monotonically as β is increased. For Figure 2(b) simple geometry shows that the ratio BC/AB is independent of β. However, since the limit of $\alpha_\sigma = 1$ can be approached but never reached by shear deformable structures, the conclusion from Figures 2(a) and 2(b) is that, for all possible values of α_n or α_σ, the error ε increases monotonically as β increases. This means that increasing the load on the structure will always result in increased percentage errors in natural frequencies calculated by neglecting shear deformation.

Similar arguments to those in the previous paragraph show that the absolute percentage correction $|\delta|(= -\delta)$ needed to obtain the shear deformable natural frequencies from

those calculated by ignoring shear deformation must also increase monotonically as the load on the structure is increased; see, e.g., equation (11).

It can be seen from Figure 1 that, as β approaches α_σ, ε ($=100 \times BC/AB$) approaches infinity and $|\delta|$ ($=100 \times BC/AC$) approaches 100%. Of course $\beta > \alpha_\sigma$ is not physically possible, because the real structure buckles when $\beta = \alpha_\sigma$. Note that the value of α_n has almost no effect on the very high values of ε and δ obtained as $\beta \to \alpha_\sigma$, and hence the average value of α_n and α_σ will not be a very good guide to the values of ε and δ in this region. Table 1 (ignoring the last four columns, which are discussed beneath equation (22)) illustrates this by using predictions of ε and δ obtained from equations (17) and (18). Note that for $\alpha_n = \alpha_\sigma = \alpha$ (say) these equations simplify to

$$\varepsilon \approx 100\left(\frac{1-\alpha}{\alpha-\beta}\right), \qquad \delta \approx -100\left(\frac{1-\alpha}{1-\beta}\right). \tag{19, 20}$$

Clearly this table gives a numerical "feel" for the behaviour of ε and δ. It takes less than one minute to obtain ε from equation (17) or δ from equation (18) if α_n and α_σ are known, and equations (19) and (20) are even easier to apply when it is assumed that α_n and α_σ are equal. Hence it is easy to obtain a numerical prediction for any problem not covered by the table.

The case $\alpha_n = \alpha_\sigma$ is of considerable practical importance. For example, a designer who knows the values of the natural frequencies of the unloaded structure with shear deflection both included and ignored can calculate α_n and hence can obtain the chain-dotted line of Figure 3 by assuming that $\alpha_\sigma = \alpha_n$. The dashed line in Figure 3 is the SDPT line shown dashed in Figure 1 and will be *assumed in this paragraph* to be the exact result for the shear deformable case. The dotted line in Figure 3 is obtained if the buckling loads are known with shear deflections both included and ignored, so that α_σ can be calculated and it is then assumed that $\alpha_n = \sigma_\sigma$. The percentage errors ε_n for the chain-dashed line and ε_σ for the dotted line are given by Figure 3 as

$$\varepsilon_n = -100 \times \frac{DB}{AB}, \qquad \varepsilon_\sigma = 100 \times \frac{BE}{AB}, \tag{21}$$

TABLE 1

Various predictions of percentage errors and percentage corrections

β	α_n	α_σ	$\frac{1}{2}(\alpha_n + \alpha_\sigma)$	ε (%)	δ (%)	ε_n (%)	ε_σ (%)	δ_n (%)	δ_σ (%)
0·00	0·90	0·96	0·93	11·11	−10·00	0·00	6·67	0·00	−6·25
0·00	0·96	0·96	0·96	4·17	−4·00	0·00	0·00	0·00	0·00
0·20	0·90	0·96	0·93	12·28	−10·94	−1·75	6·67	1·79	−6·25
0·20	0·96	0·96	0·96	5·26	−5·00	0·00	0·00	0·00	0·00
0·40	0·90	0·96	0·93	14·29	−12·50	−4·76	6·67	5·00	−6·25
0·40	0·96	0·96	0·96	7·14	−6·67	0·00	0·00	0·00	0·00
0·60	0·90	0·96	0·93	18·52	−15·63	−11·11	6·67	12·50	−6·25
0·60	0·96	0·96	0·96	11·11	−10·00	0·00	0·00	0·00	0·00
0·80	0·90	0·96	0·93	33·33	−25·00	−33·33	6·67	50·00	−6·25
0·80	0·96	0·96	0·96	25·00	−20·00	0·00	0·00	0·00	0·00
0·90	0·90	0·96	0·93	77·78	−43·75	−100·00	6·67	∞	−6·25
0·90	0·96	0·96	0·96	66·67	−40·00	0·00	0·00	0·00	0·00
0·96	0·90	0·96	0·93	∞	−100·00	−∞	—	∞	—
0·96	0·96	0·96	0·96	∞	−100·00	—	—	—	—

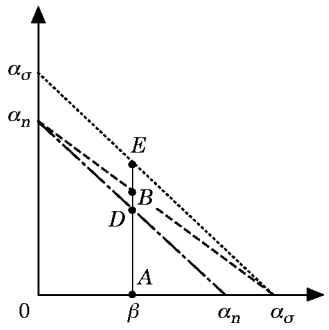

Figure 3. A comparison of the lines for the case in which shear deflection is included. ----, Taken from Figure 1; –·–, obtained when α_n is known and it is assumed that $\alpha_\sigma = \alpha_n$; ····, obtained when α_σ is known and it is assumed that $\alpha_n = \alpha_\sigma$.

where the negative sign indicates an underestimate. Similarly, the correction percentages δ_n and δ_σ are given by

$$\delta_n = 100 \times \frac{DB}{AD}, \qquad \delta_\sigma = -100 \times \frac{BE}{AE}, \tag{22}$$

where the negative sign indicates a reduction. Note that it is obvious from the geometry of Figure 3 that BE/AE and BE/AB are both constant for all values of β, so that equations (21) and (22) show that ε_σ and δ_σ do not vary with the load or stress level. It is also clear that assuming $\alpha_\sigma = \alpha_n$ gives underestimates of the loaded natural frequency for all values of β, and that assuming $\alpha_n = \alpha_\sigma$ gives overestimates for all values of β. The last four columns of Table 1 confirm these facts by giving the values of ε_n, ε_σ, δ_n and δ_σ obtained from equations (21) and (22), as can be verified by applying similar triangles to the geometry of Figure 3.

Note that to obtain numerical results for loaded natural frequencies $n_{\sigma rs}$ from the preceding paragraph it is necessary to know the CPT buckling stress σ_{rc} in the chain-dotted case, or n_{rc} in the dotted case. Alternatively, they can be obtained—either exactly or approximately depending on the problem—from equation (3).

4. RESULTS FOR AN ORTHOTROPIC PANEL

In Figure 4 are shown the geometric and lay-up details of a realistic aircraft wing panel similar to one which has previously been the subject of a parametric study [26] as part of a GARTEUR (Group for Aeronautical Research and Technology in Europe) Action Group on Structural Optimization. The material properties of each ply were as follows: $E_{11} = 125$ GPa, $E_{22} = 8{\cdot}8$ GPa, $G_{12} = G_{13} = 5{\cdot}3$ GPa, $G_{23} = 0{\cdot}5G_{13} = 2{\cdot}65$ GPa, $\nu_{12} = 0{\cdot}35$ and $\rho = 1620$ kg/m^3. The stiffener web and flange breadths, b_w and b_f, were 59·30 mm and 25·0 mm, respectively. The skin, flange and web were formed from the same symmetric $(\pm 45, 0, 90, 0, \mp 45)$ laminate with layer thicknesses of 1·697 mm and 0·207 mm for the 0° and 90° plies, respectively, and 0·786 mm for the $\pm 45^\circ$ plies. Hence, on Figure 4, $t_s = t_f = t_w = 6{\cdot}745$ mm. As the plates of the panel are almost orthotropic, the natural frequencies could be found to high accuracy by using the quick VIPASA analysis route of VICONOPT [27] in place of the "exact" VICON [28] analysis; i.e., by using a single value of λ, as assumed in this paper, rather than by coupling responses for different values of λ. (For this panel, the differences between the results given by VIPASA and VICON analyses were observed to be 0·6% or less.) These VIPASA analysis results are denoted

by using a superscript V throughout the results that follow; e.g., σ_{rc}^{V} and σ_{rs}^{V} are the buckling stresses given by VIPASA theory using CPT and SDPT, respectively.

The accuracy obtained when the unloaded CPT and SDPT natural frequencies of this panel were converted to critical buckling stresses by using equations (3) and (6) is demonstrated in Table 2. It can be seen that the percentage error, ε_c, incurred by using equation (3) to calculate the CPT critical buckling stresses from the CPT natural frequencies is zero throughout, as must be the case for a VIPASA analysis of panels with component plates with identical orthotropic properties, so that they share the same values of σ and ρ. Fortunately, and less predictably, the corresponding errors ε_s for the SDPT case are also very small ($|\varepsilon_s| \leqslant 0{\cdot}418\%$). ε_c and ε_s were calculated using values of σ_{rc}^{V} and σ_{rs}^{V} that are not shown in the table. Table 2 also gives ε_{cs}, the percentage error incurred when CPT is used instead of SDPT to find the natural frequencies of the panel; i.e., the percentage by which the value of n_{rc}^{V} in the table exceeds that of n_{rs}^{V}.

The smallest value $\varepsilon_{cs} = 0{\cdot}27\%$ occurred for the fundamental SDPT mode ($i = 1, r = 1$), while the largest value of $\varepsilon_{cs} = 6{\cdot}82\%$ occurred for the 43rd SDPT mode when $i = 7$ and $r = 4$; i.e., the fourth mode where $\lambda = \ell/7$. (This result should be interpreted with some

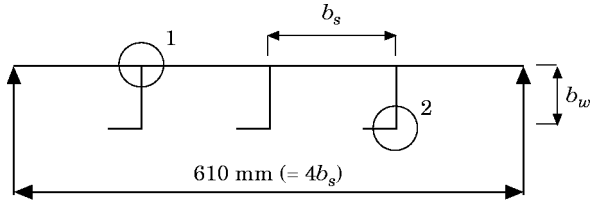

(a)

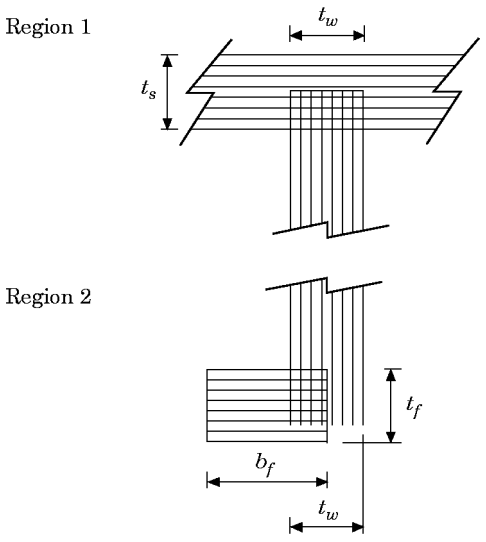

(b)

Figure 4. The stiffened aircraft wing panel analysed using VIPASA. The length of the panel is $\ell = 752$ mm. (a) Cross-section; (b) detail of regions 1 and 2 of the panel.

TABLE 2

The first 45 *natural frequencies* n^V_{rc} *and* n^V_{rs} *of the panel of Figure* 4, *showing the number of longitudinal half-waves in the mode*, $i\ (=\ell/\lambda)$, *and the critical buckling stresses*, σ_{rc} *and* σ_{rs}, *predicted by equations* (3) *and* (6). ε_c *and* ε_s *are the percentage errors*, *obtained by comparing the predicted critical buckling stresses with the correct values* (*calculated by VIPASA*), *while* ε_{cs} *is the percentage error that would be caused by using the correct CPT value instead of the correct SDPT value*

			Predicted					Predicted			
No.	i	r	n^V_{rc} (Hz)	σ_{rc} (Mn/m^2)	ε_c (%)	i	r	n^V_{rs} (Hz)	σ_{rs} (Mn/m^2)	ε_s (%)	ε_{cs} (%)
1	1	1	349·972	448·826	0·000	1	1	349·032	446·418	−0·019	0·27
2	1	2	380·919	531·710	0·000	1	2	379·773	528·518	−0·048	0·30
3	1	3	456·057	762·167	0·000	1	3	453·888	754·933	−0·107	0·48
4	1	4	566·923	1177·764	0·000	1	4	562·855	1160·923	−0·179	0·72
5	1	5	763·873	2138·225	0·000	1	5	754·444	2085·761	−0·198	1·25
6	2	1	777·114	553·249	0·000	2	1	769·614	542·621	−0·160	0·98
7	1	6	822·802	2480·855	0·000	1	6	808·118	2393·095	−0·260	1·82
8	2	2	830·462	631·815	0·000	2	2	821·098	617·648	−0·162	1·14
9	2	3	867·342	689·178	0·000	2	3	854·881	669·518	−0·122	1·46
10	2	4	943·763	815·974	0·000	2	4	923·764	781·758	−0·131	2·17
11	1	7	1077·801	4256·843	0·000	1	7	1048·592	4029·246	−0·250	2·79
12	3	1	1118·121	509·046	0·000	3	1	1094·020	487·338	−0·191	2·20
13	1	8	1167·213	4992·421	0·000	1	8	1134·303	4714·860	−0·258	2·90
14	3	2	1169·600	556·999	0·000	3	2	1138·783	528·034	−0·203	2·71
15	3	3	1253·763	640·045	0·000	3	3	1217·397	603·454	−0·174	2·99
16	2	5	1272·590	1483·637	0·000	2	5	1240·765	1410·360	−0·262	2·57
17	2	6	1292·222	1529·767	0·000	2	6	1261·301	1457·432	−0·229	2·45
18	2	7	1315·685	1585·822	0·000	3	4	1282·580	669·805	−0·146	3·26
19	3	4	1324·341	714·134	0·000	2	7	1282·832	1507·615	−0·229	2·56
20	4	1	1422·499	463·441	0·000	4	1	1379·035	435·553	−0·242	3·15
21	1	9	1435·982	7556·292	0·000	1	9	1386·439	7043·888	−0·277	3·57
22	4	2	1455·532	478·571	0·000	4	2	1397·981	447·603	−0·246	3·40
23	4	3	1569·383	564·091	0·000	4	3	1505·706	519·244	−0·231	4·23
24	4	4	1665·419	635·240	0·000	4	4	1588·489	577·909	−0·212	4·84
25	1	10	1740·272	11 098·010	0·000	1	10	1672·339	10 248·470	−0·304	4·06
26	5	1	1749·845	448·818	0·000	5	1	1685·785	416·558	−0·295	3·80
27	5	2	1763·145	455·666	0·000	5	2	1696·462	421·851	−0·295	3·93
28	2	8	1787·143	2925·967	0·000	2	8	1756·506	2826·506	−0·173	1·74
29	3	5	1787·269	1300·648	0·000	3	5	1757·185	1257·230	−0·278	1·71
30	3	6	1821·724	1351·279	0·000	3	6	1786·037	1298·855	−0·283	2·00
31	3	7	1865·434	1416·901	0·000	5	3	1799·752	474·784	−0·286	4·96
32	5	3	1888·925	522·998	0·000	3	7	1825·057	1356·228	−0·288	2·21
33	2	9	1917·005	3366·642	0·000	2	9	1875·173	3221·316	−0·222	2·23
34	5	4	1985·071	577·594	0·000	5	4	1878·276	517·118	−0·273	5·69
35	6	1	2122·961	458·743	0·000	6	1	2033·723	420·987	−0·359	4·39
36	6	2	2132·392	462·827	0·000	6	2	2041·098	424·046	−0·359	4·47
37	2	10	2163·355	4287·521	0·000	2	10	2101·774	4046·902	−0·287	2·93
38	6	3	2250·051	515·312	0·000	6	3	2132·130	462·714	−0·352	5·53
39	6	4	2338·983	556·851	0·000	6	4	2200·599	492·909	−0·341	6·29
40	7	1	2548·384	485·687	0·000	7	1	2427·278	440·621	−0·418	4·99
41	7	2	2555·768	488·505	0·000	7	2	2432·781	442·621	−0·418	5·06
42	4	5	2609·804	1559·935	0·000	7	3	2510·407	471·318	−0·411	6·08
43	4	6	2634·233	1589·275	0·000	7	4	2567·632	493·051	−0·402	6·82
44	7	3	2662·979	530·349	0·000	4	5	2568·182	1510·575	−0·319	1·62
45	4	7	2673·957	1637·569	0·000	4	6	2591·296	1537·888	−0·327	1·66

caution, because theory and experiment are likely to differ at such high frequencies.) For the $i = 1$, $r = 1$ mode, VIPASA results give $\alpha_n = 0{\cdot}9946$ and $\alpha_\sigma = 0{\cdot}9948$; while for the $i = 7$, $r = 4$ mode, $\alpha_n = 0{\cdot}8765$ and $\alpha_\sigma = 0{\cdot}8800$. (The $i = 1$, $r = 1$ values can be deduced from Table 2, but those for $i = 7$, $r = 4$ cannot, because the CPT results for this case lie outside the table.) As expected, the difference between α_n and α_σ increased with frequency and, as intuitively predicted in section 2, α_σ is larger than α_n. In Figure 5 are shown the actual, using VIPASA, and predicted, using equations (18) and (20), variations of $|\delta|$ $(= -\delta)$ with β^* for both of these modes, where

$$\beta^* = \frac{\sigma}{\sigma_c} = \beta \times \frac{\sigma_{rc}}{\sigma_c}. \tag{23}$$

β^* is used to indicate the proportion of the *fundamental* CPT critical buckling stress σ_c; i.e., of the lowest value of σ_{rc} for all values of i, that has been applied to the panel. The panels considered in this paper all happened to be governed by overall buckling when analyzed by CPT, and so the CPT fundamental critical buckling stress always occurred for the case ($i = 1$, $r = 1$), so that $\sigma_c = \sigma_{1c}$ and hence $\beta^* = \beta$ when $i = 1$, i.e., when $\lambda = \ell$.

The effect of increasing the axial load on the frequencies of the panel can be seen to be much greater when using SDPT. Thus the curve for the fundamental mode $i = r = 1$ shows that the percentage correction $|\delta| \to 100\%$ as $\beta^* \to \alpha_\sigma$, because in this case $\beta^* = \beta$ and so $\beta \to \alpha_\sigma$. This accords with the prediction made above equation (19). In contrast, for the $i = 7$, $r = 4$ mode $|\delta|$ increases from 12·35% for the unloaded case ($\beta^* = 0$) to around 60% when $\beta^* \approx \alpha_\sigma$; i.e., when the panel is just about to buckle.

Table 3 is explained in its caption and corresponds to Figure 5, except that it gives percentage errors ε instead of percentage correction factors δ. Note that the values of the *loaded* CPT frequencies $n^V_{\sigma rc}$ given in the table were found to be identical with those predicted by substituting $n_{rc} = n^V_{rc}$ in equation (12). This is because the CPT relationship between n^2 and σ is known to be exactly linear when all of the plates of a stiffened panel analyzed by VIPASA have identical orthotropic properties [22]. For example, consider the loaded CPT frequency for the $i = 7$, $r = 4$ mode when $\beta^* = 0{\cdot}9$ which, from Table 3, is 1456·190 Hz. The ratio of the CPT critical buckling stress for that mode and the fundamental CPT critical buckling stress (both of which can be obtained from the $n^V_{\sigma rc}$ for $\beta^* = 0$ given in the table by using equation (3)), was $\sigma_{rc}/\sigma_c = 1{\cdot}253326$. Hence, from

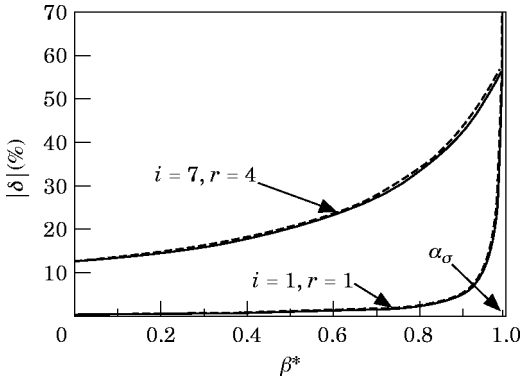

Figure 5. The variation of $|\delta|$, $= -\delta$, with β^* for the ($i = 1$, $r = 1$) and ($i = 7$, $r = 4$) modes of the panel shown in Figure 4. The curves representing the variation of $|\delta|$ predicted by equation (18) when both α_σ and α_n are known, or when α_n is assumed to be equal to α_σ, were both indistinguishable from the curve of the actual variation. —, Actual variation; -----, variation predicted by equation (20) when α_n is known and it is assumed that $\alpha_\sigma = \alpha_n$.

TABLE 3

CPT natural frequencies $n^V_{\sigma rc}$ for the panel of Figure 4 for increasing levels of axial load, and their percentage error, ε^V, relative to the SDPT natural frequencies $n^V_{\sigma rs}$. The final three columns give the error in predicting ε^V from equation (17) when α_n and α_σ are both known ($\varepsilon_{n\sigma}$), or of using equation (19) either when only α_n is known and it is assumed that $\alpha_\sigma = \alpha_n$ (ε_n) or when only α_σ is known and it is assumed that $\alpha_n = \alpha_\sigma$ (ε_σ)

Case (i, r)	β*	β	$n^V_{\sigma rc}$ (Hz)	ε^V (%)	$\varepsilon_{n\sigma}$ (%)	ε_n (%)	ε_σ (%)
1, 1	0·000	0·000	349·972	0·539	0·000	0·000	−0·009
	0·100	0·100	332·013	0·598	0·000	0·001	−0·009
	0·300	0·300	292·808	0·764	0·000	0·004	−0·009
	0·500	0·500	247·468	1·066	0·000	0·009	−0·009
	0·700	0·700	191·688	1·776	0·000	0·022	−0·009
	0·900	0·900	110·671	6·944	0·000	0·088	−0·009
	0·950	0·950	78·256	11·579	0·000	0·197	−0·009
7, 4	0·000	0·000	2742·606	14·094	0·000	0·000	−0·202
	0·100	0·080	2630·918	15·458	0·000	0·020	−0·202
	0·300	0·239	2391·949	19·208	0·000	0·076	−0·202
	0·500	0·399	2126·290	25·445	0·000	0·168	−0·202
	0·700	0·559	1822·306	37·873	0·000	0·354	−0·202
	0·900	0·718	1456·190	74·796	0·000	0·910	−0·202
	0·950	0·758	1349·225	99·116	0·000	1·282	−0·202

equation (23), $\beta = 0{\cdot}718089$, which when substituted into equation (12) predicts a loaded CPT frequency of 1456·194 Hz; i.e., 1456·190 Hz to the accuracy of the computations.

It can be seen that $\varepsilon_{n\sigma} = 0{\cdot}000$ throughout Table 3. This suggests that SDPT gave an exactly (at least for all practical purposes) linear relationship between n^2 and σ. This linearity was confirmed for the $i = 1$, $r = 1$ mode by demonstrating that VIPASA gave a value of $n^V_{\sigma 1s}$ for $\beta = 0{\cdot}5$, which was half of the value of n^V_{1s} that it gave for $\beta = 0$, to an accuracy of at least seven significant figures.

The smallness of the errors ε_n and ε_σ indicates the effectiveness of using equation (19) when either the SDPT critical buckling stress is unknown, and so α_σ cannot be determined directly, or when the SDPT unloaded frequency, and hence α_n, is unknown. As predicted beneath equation (22) in section 3, the value of ϵ_σ in the last column of the table can be seen to be constant for each of the two modes considered.

Overall, the results for the orthotropic panel of Figure 4 show that equations (3)–(7) and (17)–(20) can be variously used to predict the effect of axial load on its SDPT natural frequencies to high accuracy. The results are so accurate because all of the constituent plates were formed from the same near orthotropic laminate. Prediction of the effect of the axial load on the SDPT frequencies for panels which include anisotropy, uneven axial stress distributions and low core density is now considered.

5. RESULTS FOR LOW CORE DENSITY PANELS

The cross-section of a low core density (foam) stiffened sandwich panel, derived from one that has previously been mass optimized [25], is shown in Figure 6. The composite outer sheets had $E_{11} = 131$ GPa, $E_{22} = 13$ GPa, $G_{12} = G_{13} = 2G_{23} = 6{\cdot}41$ GPa, $v_{12} = 0{\cdot}31$ and $\rho = 1584$ kg/m^3. The foam had $E_{11} = E_{22} = 6{\cdot}89$ MPa, $G_{12} = G_{13} = G_{23} = 48{\cdot}9$ MPa, $v = 0{\cdot}0$ and density $\rho_c = 110{\cdot}6$ kg/m^3. The axial compressive load was 875·7 kN/m. The

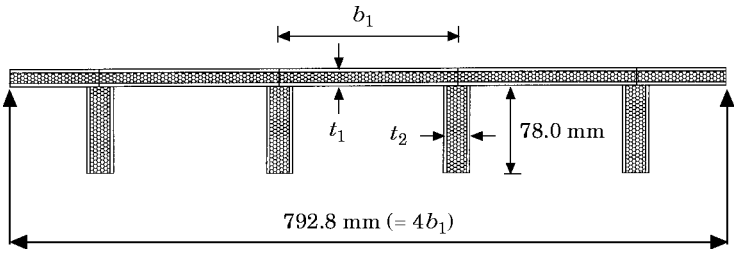

Figure 6. The cross-section of a stiffened sandwich panel of length 762 mm with low density foam cores.

outer sheets were composed entirely of 0° plies of thickness 0·666 mm for the skin and 1·148 mm for the stiffeners. The foam thicknesses were 9·940 mm for the skin and 16·800 mm for the stiffeners. Hence $t_1 = 11{\cdot}272$ mm and $t_2 = 19{\cdot}096$ mm in Figure 6. Since the skin and stiffener plates differ, their stress levels were different, and so were their average densities ρ. The stiffener stress (density) was approximately 1·75% (1·07%) higher than that of the skin. The actual plate densities were used during the VIPASA analyses, but an average panel density of 285·927 kg/m^3 was used for hand calculations; e.g., when using equations (3) and (6).

The CPT and SDPT natural frequencies n_{rc} and n_{rs} (for $r = 1$), predicted from $\bar{\sigma}^V_{rc}$ and $\bar{\sigma}^V_{rs}$ by equations (3) and (6), respectively, are listed in Table 4. Even though averaged critical buckling stresses and panel densities were used, the percentage errors ε_c and ε_s are still small, the largest being only 0·376%. However, the errors ε_{cs} incurred by using CPT instead of SDPT to find the natural frequencies are much greater; e.g., 3·6% for the fundamental mode and 39·4% for the first mode with $\lambda = \ell/3$. For the $i = 1$, $r = 1$ mode, VIPASA results gave $\alpha_n = 0{\cdot}9318$ and $\alpha_\sigma = 0{\cdot}9330$, while for the $i = 3$, $r = 1$ mode $\alpha_n = 0{\cdot}5149$ and $\alpha_\sigma = 0{\cdot}5170$. Note that $\bar{\sigma}^V_{1s}$ decreases progressively as i is increased, indicating a mode dominated by shear deformation. Moreover, the limit to which $\bar{\sigma}^V_{1s}$ is approaching is clearly less than 70·971 MN/m^2, so that since the table gives the lowest CPT buckling stress as 103·072 MN/m^2 it follows that values of β^* that exceed $70{\cdot}971/103{\cdot}072 \approx 0{\cdot}7$ give loadings above the buckling load, and so are avoided in Figure 7 and Table 5 below.

TABLE 4

The lowest CPT and SDPT average critical buckling stresses, $\bar{\sigma}^V_{1c}$ and $\bar{\sigma}^V_{1s}$ (i.e., $r = 1$) of the foam core sandwich panel of Figure 6 for the first nine values of i ($=\ell/\lambda$). The corresponding natural frequencies n_{1c} and n_{1s} predicted by equations (3) and (6) are also given plus the percentage errors ε_c and ε_s of the predicted natural frequencies compared with the "correct" values n^V_{1c} and n^V_{1s} given by VIPASA

	Predicted			Predicted			
i	$\bar{\sigma}^V_{1c}$ (MN/m^2)	n_{1c} (Hz)	ε_c (%)	$\bar{\sigma}^V_{1s}$ (MN/m^2)	n_{1s} (Hz)	ε_s (%)	ε_{cs} (%)
1	103·072	393·965	0·010	96·168	380·542	0·077	3·6
2	135·348	902·909	0·032	92·758	747·468	0·376	21·2
3	155·616	1452·231	0·105	80·446	1044·143	0·305	39·4
4	190·884	2144·531	0·128	78·527	1375·491	0·279	56·1
5	246·163	3044·168	0·130	78·913	1723·576	0·258	76·8
6	320·613	4168·973	0·131	78·338	2060·746	0·240	102·5
7	412·741	5518·395	0·128	76·419	2374·508	0·221	132·6
8	521·084	7086·493	0·129	73·762	2666·199	0·212	166·0
9	643·961	8862·536	0·121	70·971	2942·183	0·203	201·5

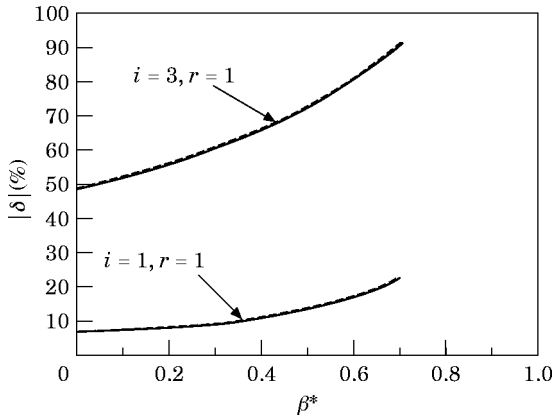

Figure 7. The variation of $|\delta|$; $= -\delta$, with β^* for the ($i = 1$, $r = 1$) and ($i = 3$, $r = 1$) modes of the panel shown in Figure 6. The curves representing the variation of $|\delta|$ predicted by equation (18) when both α_σ and α_n are known, or when α_n is assumed to be equal to α_σ, were both indistinguishable from the curve of the actual variation. —, Actual variation; -----, variation predicted by equation (20) when α_n is known and it is assumed that $\alpha_\sigma = \alpha_n$.

In Figure 7 is shown the variation of $|\delta|$ as the axial load factor β^* is increased for the fundamental and $i = 3$, $r = 1$ modes. Clearly, $|\delta|$ is now much larger for all β^* than for the panel results of Figure 5 due to the foam. The actual percentage error, ε^V, that would be incurred if CPT were used in place of SDPT to find the loaded natural frequencies for the fundamental mode and the $i = 3$, $r = 1$ modes is shown in Table 5. It can be seen that the effect of axial load on the SDPT frequencies is much greater than for the CPT frequencies. Thus for the fundamental mode when $\beta^* = 0$ the percentage error is 7·324%, rising to 28·92% when $\beta^* = 0{\cdot}7$, whereas for the shorter half-wavelength mode the errors were (as expected) much greater. However, the percentage errors in estimating ε^V from the loaded CPT frequencies by using equation (17) when both α_n and α_σ are known exactly, $\varepsilon_{n\sigma}$, or by using equation (19) when either of α_n or α_σ is known, are very small.

In order to increase the unequal stress distribution between the skin and the stiffeners an anisotropic ($\pm 45_5$) lay-up with $t_{45} = 0{\cdot}0666$ mm was used instead of the 0° plies of the skin cover plates, while the stiffener cover plates became ($\pm 45, 0, \mp 45$) with $t_0 = 16t_{45} = 0{\cdot}9184$ mm. Hence the thicknesses and densities of the skin and stiffener plates

TABLE 5

Results for the panel of Figure 6, *with all symbols having the meanings given in the caption of Table* 3

Case (i, r)	β^*	β	$n^V_{\sigma rc}$ (Hz)	ε^V (%)	$\varepsilon_{n\sigma}$ (%)	ε_n (%)	ε_σ (%)
1, 1	0·000	0·000	393·927	7·324	0·000	0·000	−0·068
	0·100	0·100	373·712	8·187	0·000	0·008	−0·067
	0·300	0·300	329·583	10·731	0·000	0·032	−0·067
	0·500	0·500	278·549	15·625	0·000	0·078	−0·067
	0·700	0·700	215·763	28·920	0·000	0·204	−0·067
3, 1	0·000	0·000	1450·707	94·217	0·000	0·000	−0·200
	0·100	0·066	1401·840	108·004	0·000	0·030	−0·199
	0·300	0·199	1298·602	152·793	0·000	0·126	−0·199
	0·500	0·331	1186·414	261·459	0·001	0·359	−0·199
	0·700	0·464	1062·445	910·208	0·001	1·789	−0·198

remained the same, but now the stress in the stiffener plates was 5·078 *times greater* than that in the skin plates. The linearity of the relationship between n^2 and σ for the $i = 1$, $r = 1$ and $i = 3$, $r = 1$ modes was again checked by using VIPASA, and the predicted and actual values of the frequency at $\beta^* = 0{\cdot}5$ were found to be within 0·272% and 2·257% of each other, respectively. The curves of the actual variation of $|\delta|$ and of that predicted by equation (18) for the $i = 3$, $r = 1$ mode were now found to be distinct, but even for this highly unrealistic panel the largest difference between the actual loaded SDPT frequencies $n^V_{\sigma rs}$ and those predicted from the loaded CPT frequencies was never larger than $-0{\cdot}23\%$ and 6·0% for the $i = 1$, $r = 1$ and $i = 3$, $r = 1$ modes, respectively.

6. CONCLUSIONS

Many structures have a linear or approximately linear relationship between natural frequencies squared and load factor both with and without shear deformation included. Hence the equations presented enable prediction and/or correction of errors caused by neglecting shear deformation when calculating natural frequencies under load. The principal equations are equations (17)–(22), which are very simple to apply and yield Table 1, which is adequate for qualitative and many approximate quantitative purposes all the way up to the elastic buckling load. An important insight is given into why, and how dramatically, the errors caused by neglecting shear deformation grow with increasing load.

Uses of the equations presented include the following. If the unloaded natural frequencies and corresponding buckling loads are known both with and without shear deformation included, then the error for that problem *and similar problems* caused by calculating loaded natural frequencies with shear deformation neglected can be predicted reasonably accurately. Alternatively, the natural frequencies of the loaded structure, including shear deformation, can be predicted to good accuracy. They can also be predicted somewhat less accurately if either the shear deformable unloaded natural frequency or buckling load is unknown.

The usefulness of the methods presented for uniform compression problems has been demonstrated by applying them to a stiffened aerospace panel consisting of a prismatic assembly of laminated plates and to two stiffened sandwich panels with very low core densities and shear stiffnesses, one of which was designed such that the stiffener stress was five times that of the skin. The natural frequencies calculated from one or both of the unloaded natural frequency and buckling load with shear deformation included were always good. This contrasts with the much poorer accuracy achieved by simply using classical plate theory to obtain the natural frequencies of such uniformly compressed panels.

ACKNOWLEDGMENT

This work was funded under EPSRC grant GR/J79423.

REFERENCES

1. Ch. Massonnet 1940 *Bulletin des Cours et des Laboratoires d'Essais des Constructions du Genie Civil et d'Hydraulique Fluvial* **1**, 1–353. Les relations entre les modes normaux de vibration et la stabilite des systems elastiques.
2. A. E. Galef 1968 *Journal of the Acoustical Society of America* **44**(8), 643. Bending frequencies of compressed beams.

3. G. Fauconneau and W. M. Laird 1967 *Journal of Mechanical Engineering Science* **9**(2), 149–155. Bounds for the natural frequencies of a simply supported beam carrying a uniformly distributed axial load.
4. D. F. Pilkington and J. B. Carr 1970 *Journal of Mechanical Engineering Science* **12**(1), 70–72. Vibration of beams subjected to end and axially distributed loading.
5. W. P. Howson and F. W. Williams 1973 *Journal of Sound and Vibration* **26**, 503–515. Natural frequencies of frames with axially loaded Timoshenko members.
6. A. Bokaian 1988 *Journal of Sound and Vibration* **126**, 49–65. Natural frequencies of beams under compressive axial loads.
7. N. G. Stephen 1989 *Journal of Sound and Vibration* **131**, 345–350. Beam vibration under compressive axial load—upper and lower bound approximation.
8. S. R. Soni and C. L. Amba Rao 1974 *Computers & Structures* **4**(5), 1105–1115. Vibrations of orthotropic rectangular plates under inplane forces.
9. S. F. Bassily and S. M. Dickinson 1978 *Journal of Sound and Vibration* **59**, 1–14. Buckling and vibration of in-plane loaded plates treated by a unified Ritz approach.
10. L. Diez, C. E. Gianetti and P. A. A. Laura 1978 *Journal of Sound and Vibration* **59**, 503–509. A note on transverse vibrations of rectangular plates subject to in-plane normal and shear forces.
11. B. Tabarrok, R. G. Fenton and A. M. Elsaie 1987 *Journal of Sound and Vibration* **112**, 295–303. Lateral vibration of square plates subject to in-plane loadings.
12. G. B. Warburton 1987 *Journal of Sound and Vibration* **118**, 545–548. Comment on "Lateral vibration of square plates subject to in-plane loadings".
13. B. Attaf and L. Hollaway 1990 *Composites* **21**(2), 117–126. Vibrational analyses of stiffened and unstiffened composite plates subjected to in-plane loads.
14. H. P. Lee and S. P. Lim 1992 *Computers and Structures* **43**(3), 431–437. Free vibration of isotropic and orthotropic square plates with square cutouts subjected to in-plane forces.
15. K. M. Liew and C. M. Wang 1993 *Transactions of the American Society of Mechanical Engineers*, *Journal of Vibration and Acoustics* **115**(4), 441–447. Flexural vibration of in-plane loaded plates with straight line/curved internal supports.
16. E. J. Brunelle and S. R. Robertson 1976 *Journal of Sound and Vibration* **45**, 405–416. Vibrations of an initially stressed thick plate.
17. O. L. Roufaeil and D. J. Dawe 1982 *Journal of Sound and Vibration* **85**, 263–275. Rayleigh–Ritz vibration analysis of rectangular Mindlin plates subjected to membrane stresses.
18. L. W. Chen and J. L. Doong 1983 *Journal of Sound and Vibration* **89**, 499–508. Large amplitude vibration of an initially stressed moderately thick plate.
19. J. L. Doong 1987 *Journal of Sound and Vibration* **113**, 425–440. Vibration and stability of an initially stressed thick plate according to a high-order deformation theory.
20. K. M. Liew, Y. Xiang and S. Kitipornchai 1993 *Computers and Structures* **49**(1), 69–78. Transverse vibration of thick rectangular plates—IV. Influence of isotropic in-plane pressure.
21. W. H. Wittrick 1985 *International Journal of Mechanical Sciences* **27**(6), 375–382. Some observations on the dynamic equations of prismatic members in compression.
22. F. W. Williams, P. N. Bennett and D. Kennedy 1996 *Journal of Sound and Vibration* **194**, 13–24. Curves for natural frequencies of axially compressed prismatic plate assemblies.
23. F. W. Williams, P. N. Bennett and D. Kennedy 1996 *Proceedings of the ESA International Workshop on Advanced Mathematical Methods in the Dynamics of Flexible Bodies*, to appear. Theory, Software and new results for vibration of prismatic plate assemblies.
24. W. H. Wittrick 1968 *International Journal of Mechanical Sciences* **10**, 949–966. General sinusoidal stiffness matrices for buckling and vibration analyses of thin flat walled structures.
25. M. S. Anderson and D. Kennedy 1993 *American Institute of Aeronautics and Astronautics Journal* **31**(10), 1963–1965. Transverse shear deformation in exact buckling and vibration of composite plate assemblies.
26. C. B. York, F. W. Williams, D. Kennedy and R. Butler 1993 *Composites Engineering* **3**(7), 619–632. A parametric study of optimum designs for benchmark stiffened wing panels.
27. W. H. Wittrick and F. W. Williams 1974 *International Journal of Mechanical Sciences* **16**(4), 209–239. Buckling and vibration of anisotropic or isotropic plate assemblies under combined loadings.
28. M. S. Anderson, F. W. Williams and C. J. Wright 1983 *International Journal of Mechanical Sciences* **25**(8), 585–596. Buckling and vibration of any prismatic assembly of shear and compression loaded anisotropic plates with an arbitrary supporting structure.

APPENDIX: NOTATION

i $=\ell/\lambda$, integer number of longitudinal half-wavelengths λ in plate assembly mode
ℓ panel length
n natural frequency of free vibration
α_n $=n_{rs}^2/n_{rc}^2$, ratio of the square of an unloaded natural frequency with shear deflection included or ignored
α_σ $=\sigma_{rs}/\sigma_{rc}$, ratio of a critical buckling load factor or stress with shear deflection included or ignored
β $=\sigma/\sigma_{rc}$, load factor or stress relative to its buckling value for the same mode
β^* $=\sigma/\sigma_c$, load factor or stress relative to its lowest buckling value for any mode
δ percentage correction needed to adjust for shear deformation; see equations (18) and (20)
δ_n percentage correction needed due to setting $\alpha_\sigma = \alpha_n$
δ_σ percentage correction needed due to setting $\alpha_n = \alpha_\sigma$
ε percentage error from ignoring shear deformation; see equations (17) and (19)
ε_c percentage error when using equation (3) to predict σ_{rc} from n_{rc}
ε_n percentage error from setting $\alpha_\sigma = \alpha_n$
ε_s percentage error when using equation (6) to predict σ_{rs} from n_{rs}
ε_σ percentage error from setting $\alpha_n = \alpha_\sigma$
λ $=\ell/i$, half-wavelength
ρ density
σ load factor or uniform longitudinal compressive stress
σ_c fundamental critical buckling load factor or stress

Superscript

V "exact" VIPASA result

Subscripts

c shear deflection ignored; e.g., CPT for plates
r denotes rth critical value (for a given λ for plate structures)
s shear deflection included; e.g., SDPT for plates
σ denotes load or longitudinal compressive stress present